communications earth & environment

Article

https://doi.org/10.1038/s43247-024-01262-5

Rainfall variability increased with warming in northern Queensland, Australia, over the past 280 years

Kelsey A. Dyez [1] ✉, Julia E. Cole [1] & Janice M. Lough[2]

Floods and droughts are hydrological extremes that impact ecosystems, agriculture, and human well-being. These extremes are expected to intensify in a warmer world, although many regions lack the observations needed to place current trends in the context of long-term variability. Here we present a new multi-century record of tropical rainfall based on a multi-proxy approach from northern Great Barrier Reef coral. The robust calibration with instrumental rainfall allows us to quantitatively estimate summer rainfall in northern Queensland back to 1746 CE. We find that as global climate warmed, wet-season rainfall in this region has increased by ~10% since 1750 and the standard deviation (21-yr 1-σ) of wet-season rainfall more than doubled, as rainy years became much wetter, while dry years remained dry. Reconstructed rainfall correlates with El Niño indices and the link to Pacific temperature variability has strengthened as climate warmed, consistent with expected intensification of La Niña-related rainfall.

At a global scale, warming temperatures result in precipitation changes that lead to stronger storms that can damage human and natural systems and overwhelm flood control measures[1–3]. Understanding the regional responses of hydroclimate to warming is needed to manage such extremes. In northern tropical Queensland, rainfall is concentrated in the summer season, but annual rainfall totals vary greatly from year to year. The latest CMIP6 climate models predict that northern Australian precipitation will increase in the next century[4,5] although uncertainty in precipitation variance remains high for northeast Australia in particular[6]. Here we present a multi-century, multi-proxy reconstruction of rainfall variability in northern Queensland in the context of 20th century instrumental observations[7,8]. This record extends the geographic range of multi-century hydrologic reconstructions from farther south along the Great Barrier Reef[9,10] into the tropics, where ENSO and the monsoon are more influential and where long rainfall records are historically lacking. This robust, quantitative reconstruction provides a new baseline from which to document unprecedented change in tropical Australian rainfall over the past quarter of a millennium.

Active monsoonal conditions and tropical cyclones deliver rainy-season water vapor to the northeastern coast of Queensland from warm tropical Pacific waters and along storm tracks originating in the Austral-Asian monsoon[11,12]. After precipitating, this water transports nutrients, organic material, and sediments to the Great Barrier Reef[13]. Here we reconstruct summer rainfall via proxies sensitive to rainfall and hydrological discharge to the coast, which carries geochemical signals that are recorded in the carbonate skeletons of long-lived corals growing nearshore. We analyze a core from a massive *Porites* (spp) colony collected in 1986 from the northern Great Barrier Reef, at the mouth of the Jeannie River (14.66°S, 144.93°E, Fig. 1). This river drains a catchment of >3600 km^2; the catchment consists almost entirely of natural conservation areas[14].

In this coral core, we measured skeletal Ba/Ca, $\delta^{13}C$, $\delta^{18}O$, and Sr/Ca at 0.75 mm resolution downcore, yielding 3691 samples spanning 1746–1984. We used image processing methods to quantify luminescence along the exact sampling transects of the geochemical measurements, yielding directly comparable data. For the rainfall calibration, we develop indices of summer rainfall and runoff from stations in the catchments surrounding Jeannie River. See "Methods" for details.

We employ four rainfall proxies (Ba/Ca, $\delta^{13}C$, $\delta^{18}O$, and luminescence) that each trace overlapping aspects of the coastal hydrological cycle. The skeletal Ba/Ca ratio tracks ambient seawater [Ba][15,16]. Rivers transport Ba into coastal waters[17]; thus, Ba/Ca in skeletal coral is often used as a tracer for terrestrial runoff[18]. At Jeannie River, we find no support for complicating factors identified elsewhere, e.g., land use change[10], upwelling[19], or physiological processes that produce anomalous Ba/Ca spikes[20]. Luminescent bands in nearshore coral skeletons are most likely to result from terrestrial organic matter transported by river flow[9,21–24]. Rivers also export low-$\delta^{13}C$ DIC waters[25,26] that can be incorporated into the coral skeletal material[27];

[1]Earth and Environmental Sciences, University of Michigan, Ann Arbor, MI, USA. [2]Australian Institute of Marine Science, Townsville, QLD, Australia.
✉e-mail: kdyez@umich.edu

rainy years may further reduce skeletal $\delta^{13}C$ if cloudiness reduces photosynthesis and imparts a more negative $\delta^{13}C$ signal to the skeleton[28]. Lastly, reconstructed $\delta^{18}O_{sw}$—using paired coral Sr/Ca and $\delta^{18}O$ values[29,30]—reflects the fresher, low-$\delta^{18}O$ input from rainfall and runoff[30,31]. Although coral proxies may have multiple interpretations, in this case, the strong correlations of each proxy with rainfall and runoff data suggest that the dominant influence here is hydroclimatic.

Results and discussion

Here we present records of four hydrological proxies from the same core that date to 1746 CE, based on seasonal cycles in Sr/Ca and luminescent banding (see Methods). All geochemical measurements derive from the same powdered samples, and luminescence is measured on the identical transect used for geochemistry (Supplemental Figs. 1–4); thus, age models for all proxies are identical. These records are among the first direct comparisons between coral luminescence and multivariate geochemistry at ~monthly resolution across multi-century timescales. This approach reduces the noise inherent in each individual proxy and provides a measure of replication insofar as the proxies (and their confounding influences) are quasi-independent.

Summer (Dec-Apr; DJFMA) instrumental rainfall, derived from 16 local meteorological stations, significantly correlates ($p < 0.001$) with each individual proxy over the period 1950–1984 (Fig. 2, Supplemental Figs. 5–7, Supplemental Tables 1–2). Each proxy series also significantly correlates with the others ($p < 0.001$; Supplemental Table 3). We average the rainfall amount predicted by each of these four proxies (weighted by correlation coefficient with instrumental rainfall over 1950–1984) to obtain a single multi-proxy reconstruction of north Queensland rainfall (Fig. 3). This 4-proxy reconstruction correlates remarkably well with instrumental rainfall at r = 0.86 (WLS, $p < 0.005$). In addition, a calibration-validation model using only the even years for calibration and odd years for validation (or vice versa) shows that our rainfall reconstruction is robust to the calibration period (Methods; Supplemental Table 1).

The range in observed summer rainfall from a "drought" year (<25th percentile; <1050 mm) to a "flood" year (>75th percentile; >1720 mm) at this location is >670 mm. The uncertainty in our reconstructed rainfall estimate is ±170 mm, calculated as the average of the absolute difference between predicted and actual rainfall for each year in the period 1950–1984. The likelihood of this method mistaking a drought year for a flood year (or vice versa) is <0.5% (>3-σ).

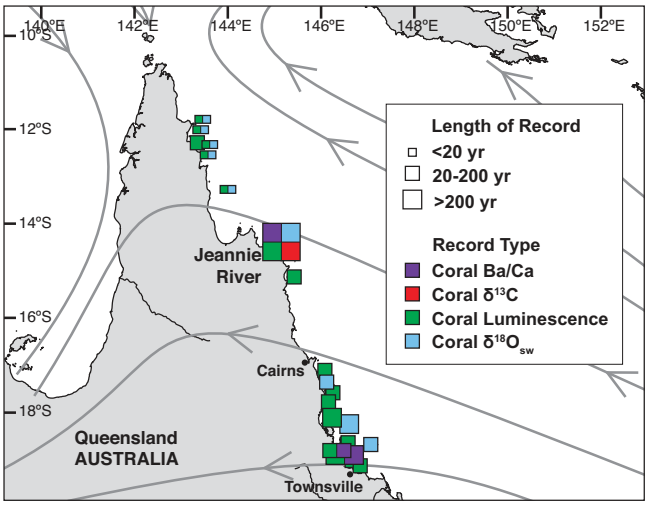

Fig. 1 | Previous work from Cape York Peninsula in Far North Queensland. The coral location is at the mouth of the ~40-km long Jeannie River that empties into the nearshore Great Barrier Reef. Other coral-based hydrological records are to the north[64] and to the south[9,10,29] of Jeannie River. Superimposed stream lines are average summer (Dec-Mar) surface wind from reanalysis of ERAinterim[65].

Rain records

This robust quantitative rainfall reconstruction allows us to explore important spatial correlations and temporal changes. Here we show that the reconstruction reflects broader NE Queensland rainfall, and explore links to decadal climate variability, assess relationships with Pacific SST patterns, show that tropical Queensland rainfall is becoming more variable as climate warms, and finally consider the implications for future warming. First, how representative of larger-scale rainfall is this precipitation record from a single location? Annual rainfall varies widely across Australia, from as little as <300 mm/yr in the interior up to >2000 mm/yr at locations in the tropical

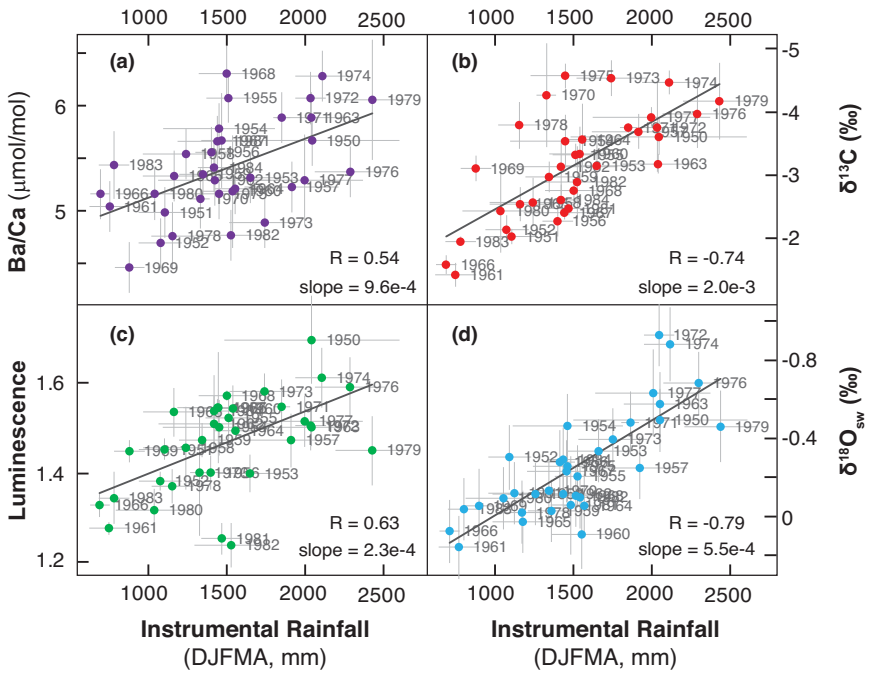

Fig. 2 | Individual proxy correlations with observed summer total rainfall. a–d Proxy uncertainty is the measurement 1-σ. Instrumental rainfall uncertainty is the 1-σ of the set of DJFMA rainfall observations available for a given year. Slopes are given in proxy units (indicated on vertical axes) per mm rainfall.

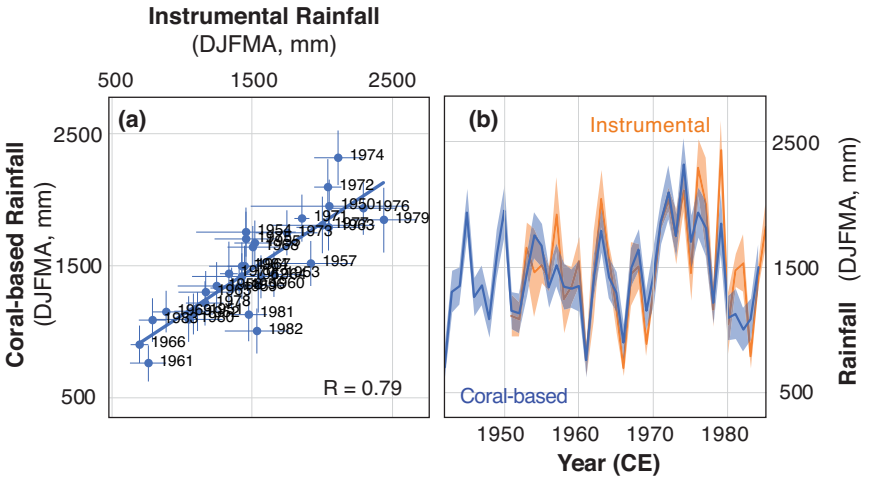

Fig. 3 | Coral multi-proxy correlation with observed summer rainfall. a Crossplot with annual 1-σ uncertainty. **b** Reconstructed rainfall from coral (blue, 1943-1984) and the instrumental record (orange, 1950–2020). The calibration set is the overlapping period 1950–1984. Blue shading is the annual 1-σ uncertainty and orange shading is the standard deviation of observed rainfall estimates among sites for a given season.

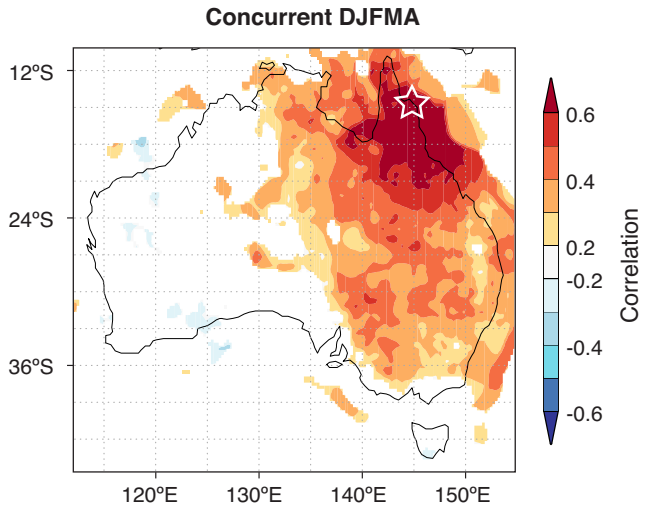

Fig. 4 | Rain correlation with Jeannie River precipitation. Correlation of DJFMA Australian instrumental rainfall[32] (AWAP, 1900–1984) with DJFMA rainfall estimates from the Jeannie River coral (star). Reconstructed precipitation reflects Queensland and eastern Australian rainfall. Figure made using KNMI Climate Explorer[66]. www.climexp.knmi.nl.

northeast[32]. The Jeannie River rainfall record most strongly correlates with wet-season rainfall throughout Queensland and the eastern half of Australia (Fig. 4). Precipitation in this region is the result of tropical climate dynamics that affect the eastern half of the continent, primarily the atmospheric circulation systems to the north and east of the continent[33].

Increase in precipitation variability

Climate models suggest that precipitation is increasing in both amount and intensity as global temperatures warm[34]. Instrumental observations validate intensifying precipitation in northern Australia in the twentieth century[35] and show that the late 20th-century warming trend in the SW Pacific has increased the likelihood of more extreme northeast Australian flooding[33]. The multivariate Jeannie River rainfall record extends the northern Great Barrier Reef pre-industrial baseline to 1746 CE and shows that average wet-season precipitation has increased by 125 mm (10%) since 1746 (Fig. 5, Supplemental Fig. 8). More dramatically, precipitation variability in northern Queensland has more than doubled since 1850 CE (110% increase in the standard deviation of summer rainfall from 21-yr windows centered on 1850–2007; Fig. 6). Increasing variability is consistent with amplified precipitation extremes in the tropics as the climate warms; global temperature has increased by ~1.1 K from 1850 to 2017, and local temperature at Jeannie River has increased by a similar amount[36].

Interannual and decadal variability

On interannual scales, El Niño and La Niña events are associated with differences in northeast Australian precipitation[8,12]. Here we resolve the degree of influence of ENSO on rainfall in northern Queensland via annual correlations between Pacific indices and the multi-proxy rainfall record (Supplemental Tables 4–5). For these analyses, we use observations and proxy-based records of ENSO[37,38]. The reconstructed Jeannie River rainfall correlates significantly with ENSO indices; the La Niña phase is associated with increased rainfall and El Nino with reduced rainfall (Supplemental Table 5). Climate models agree that rainfall associated with ENSO will likely intensify in the coming decades[4,39] regardless of the trend in ENSO SST variability[40]. Indeed, over the period 1870–2021, the linkage between reconstructed north Queensland rainfall and ENSO strengthens (Supplemental Fig. 9).

Interannual (ENSO) relationships are further modulated by Pacific decadal variability, which is described by the decadal SST-based indices TPI, SOI, IPO, and PDO (see Methods; Supplemental Table 4). The Jeannie River rainfall record is coherent with Pacific decadal SST variability, which influences precipitation variability throughout the tropical Pacific[41]. The link between ENSO and north Queensland rainfall is stronger when the IPO (or TPI) is negative[42]. This leads rainfall to often be greatest when La Niña and negative IPO coincide[12,41]. In fact, once we remove El Niño-scale variability from the records (low-pass >8 yr filter), the decadal-scale IPO index is the best explanation of the remaining variance in rainfall (Supplemental Tables 4–5).

Spatial rainfall correlations

We also find significant correlations between Jeannie River rainfall and the southwest Pacific SST field, for the months prior to the rainy season. Especially rainy summer seasons tend to be preceded by anomalously warmer SST that gradually moves from the region between New Zealand and the equator (the South Pacific Convergence Zone; SPCZ) towards the coast (Fig. 7). Warmer SPCZ SST provides additional water vapor to be transported towards Queensland. In contrast, dry years in Queensland are preceded by cooler SST anomalies. The area associated most closely with northern Queensland rainfall is the southern edge of the SPCZ (Fig. 7), where equatorial moisture sources encounter a large-scale Rossby wave emanating from the Southern Ocean over southeast Australia[43].

We further confirm the relationship between interannual Queensland rainfall and the spring SST field by comparing Jeannie River rainfall with coral-based SST records from the heart of the SPCZ (Supplemental Figs. 10–11): New Caledonia[44], Fiji, and Rarotonga[45]. All three of these coral-based SST records are well correlated ($p < 0.05$) with local SST over the

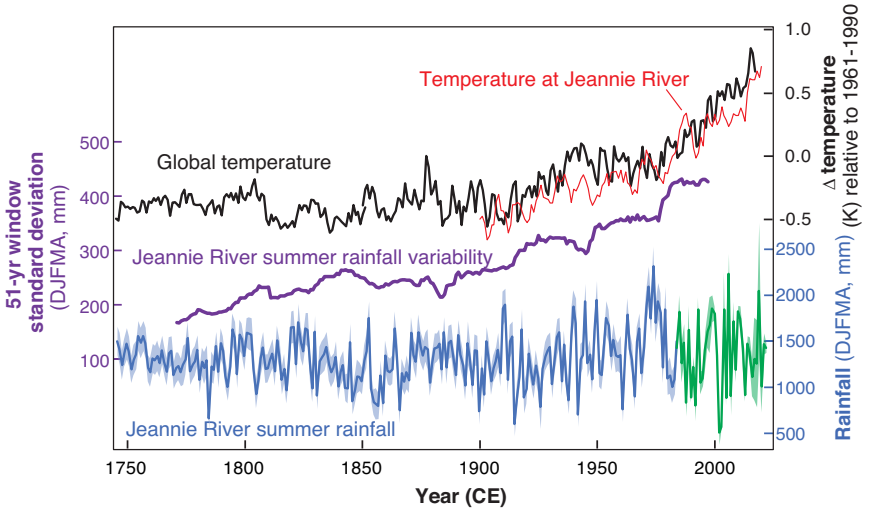

Fig. 5 | Increasing summer rain variability. Jeannie River summer rainfall variability (51-yr running standard deviation, purple line) increased from the mid-18th century to 21st century as global temperature (black line) increased[67]. Blue line is the multi-proxy rainfall reconstruction of DJFMA total rainfall 1746–1984 with 1-σ uncertainty; rainfall after 1984 is instrumental (green). Red line: surface temperature at Jeannie River (HadCRUT5, 5-yr mean, 1900–2020)[36].

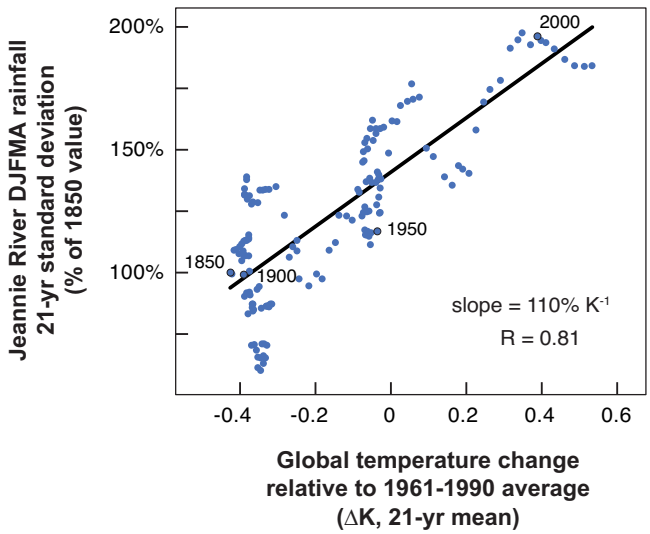

Fig. 6 | Change in rainfall variability since 1850. Each value is the percent change in standard deviation of DJFMA total rainfall vs global temperature change relative to the 1961–1990 average[67] for 21-yr windows centered on years 1850–2007 CE. The slope of the relationship is 110% per degree K. Alternatively, the same exercise using longer time windows (e.g. 31-yr or 51-yr, not shown) demonstrate that rare events are also becoming more extreme (120% and 125% change in standard deviation of DJFMA rainfall per degree warming since 1850, respectively).

instrumental period[46]. We find that preceding-season coral-based SSTs are correlated with Jeannie River rainfall from the 1700s onward (Supplemental Table 5). Thus, we suggest that summer rainfall on the northeast coast of Queensland is 'primed' by additional atmospheric water vapor—resulting from warm spring SST in the southwest Pacific in the months preceding the rainy season—and has been over the past 250 years. While the correlation is lower as we expand the time window to include older material, this could simply be a result of age model offsets in the older portion of the records.

This record complements studies that use a single variable to estimate rainfall from many locations[9,47] and those that are further south in the Great Barrier Reef[10]. The history of rainfall variability in this multivariate record agrees in broad strokes with that based on luminescence from multiple cores (Supplemental Fig. 12). However, variability in the luminescence-only record from multiple cores could theoretically have included a bias from age model misalignments that would serve to smooth evidence of extreme events further back in time. The Jeannie River record precludes this bias yet nevertheless indicates that rainfall variability has increased. Others have suggested that increasingly variable coral Ba/Ca near the Burdekin River (~18°S) represented land-use changes brought on by European settlement[10]. Our record (from a minimally developed catchment) suggests that increasing rainfall variability may contribute to increased Ba/Ca in Great Barrier Reef skeletal coral, in addition to any anthropogenic land-use changes in the upstream catchments.

Implications

Our new, quantitative rainfall reconstruction for northern Queensland reveals an unprecedented increase in rainfall variability concurrent with global and regional warming, alongside an increase of ~10% in wet-season rainfall amount. As interannual variability intensifies, the correlation to ENSO becomes increasingly strong, as anticipated by model projections for future climate[4,40,41].

As global temperatures continue to warm, the impacts of intensifying tropical rainfall variability are particularly relevant for human society. In the 18th and 19th centuries, tropical Queensland summers were less rainy and less variable year-to-year. Over the 20th century, Queensland rainfall became increasingly intense and variable. The unprecedented nature of such increased precipitation and rainfall variability suggests that communities in tropical locations re-evaluate the capacity of infrastructure that will be needed to manage increasing precipitation variability in the decades to come as the global climate system continues to warm.

Methods

The coral material used in this study is from the Australian Institute of Marine Science's (AIMS) archive of long coral cores from the Great Barrier Reef[9,48]. We analyzed one core, "JNE" (JNE01A, 14.66°S, 144.93°E, 3 m water depth), from a *Porites* colony collected in 1986 near the Jeannie River, which flows through Cape York Peninsula Aboriginal land. Core slabs (~7 mm thick) were taken along the main growth axis, analyzed for luminescence[9,48] and X-rayed (Supplemental Fig. 1). For geochemical samples, we micro-milled samples at 0.75 mm resolution along the axis of maximum growth and avoided 'trough'-like areas, cracks, and holes. Transects are ~5 mm wide and ~2 mm deep. A total of 3691 samples were collected and analyzed from 37 transects for stable isotopes, Sr/Ca, Mg/Ca, and Ba/Ca (Supplemental Fig. 1, summary of annual monthly averages in Supplemental Fig. 3).

Elemental analysis

We measured elemental concentrations of Sr, Ca, Mg, and Ba using a Thermo iCAP 7400 inductively coupled plasma optical emission spectrometer (ICP-OES) in the PACE lab at the University of Michigan's Earth and

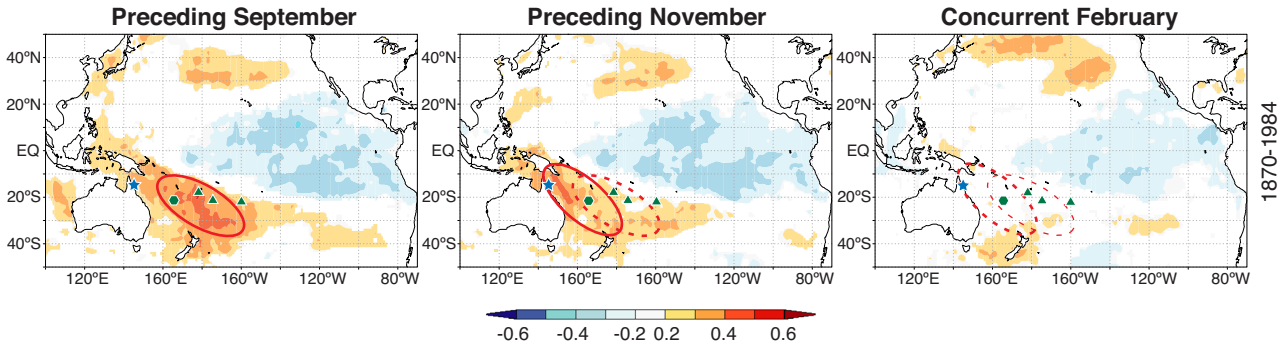

Fig. 7 | Rainfall is related to SPCZ temperature. Monthly correlation (r) of HadlSST1 (1870-1984) with summer (DJFMA) rainfall at Jeannie River (blue star) in preceding September (**a**), preceding November (**b**), and concurrent February (**c**). Positive SST correlation with Queensland rainfall builds in the preceding Aug–Dec and moves toward the coast through the austral spring. Positive rainfall correlation with SST breaks down in austral summer and fall. North Queensland rainfall is negatively correlated with central tropical Pacific SST, i.e., the region is wetter in more 'La-Niña'-like years. Green hexagon is New Caledonia, green triangles are Fiji, Tonga, and Rarotonga (from west to east). Figure made using KNMI Climate Explorer[66]. www.climexp.knmi.nl.

Environmental Science department using established methods[49,50]. For each carbonate sample split, 400–600 µg samples were diluted to [Ca] ~ 80 ppm in 3.5 ml of 5% trace metal grade HNO_3. Six calibration solutions spanning the expected elemental concentrations were analyzed at the start of each day of analysis. A reference solution was measured every 3rd sample to correct within-run drift, another reference solution (MCP-L) was measured 10 times per day to correct for day-to-day offsets, and two powdered internal standards were analyzed each day of analysis to monitor long-term elemental values. Long-term analytical precision (1-σ) of the first internal standard (MCP-P) was Sr/Ca = 0.018 mmol/mol, Mg/Ca = 0.055 mmol/mol, and Ba/Ca = 0.24 µmol/mol (1-σ, $n = 114$). The long-term average values of the second powdered coral standard (JCp-1) were Sr/Ca = 8.861 ± 0.026 mmol/mol, Mg/Ca = 4.141 ± 0.091 mmol/mol, and Ba/Ca = 6.70 ± 0.41 µmol/mol (1-σ, $n = 136$), within 1-σ of previous measurements[49,51].

Stable isotope geochemistry

We analyzed stable oxygen and carbon isotope ratios ($\delta^{18}O$ and $\delta^{13}C$) using a Thermo Delta V Plus mass spectrometer, coupled to a Kiel IV carbonate preparation system in the PACE lab, at the University of Michigan's Earth and Environmental Science department. Output values were calibrated using the NIST standard carbonate materials NBS 19 and NBS 18. These samples were splits of the same powders analyzed for elemental chemistry. The long-term average values of a Luxor internal carbonate standard were $\delta^{18}O = -9.08 \pm 0.08$‰ and $\delta^{13}C = -1.19 \pm 0.05$‰ (1-σ, $n = 249$).

We used established methods and slopes for deriving $\delta^{18}O_{sw}$ from coral Sr/Ca and $\delta^{18}O$[31]:

$$\delta^{18}O_{sw} = \left(\left[\delta^{18}O_c - \delta^{18}O_{average}\right] - k_1 * \left[\left((Sr/Ca) - (Sr/Ca)_{average}/k_3\right)\right]\right) * k_2$$

where k_1 is −0.21 permil / °C, $k_2 = 1$ (unknown, but must be a constant), and k_3 is −0.062 mmol/mol per °C. The slope of k_3 is in agreement with other recent estimates from Great Barrier Reef coral (−0.05 to −0.08 mmol/mol/C°)[52]; this method has the advantage of not requiring an absolute SST value as part of the calculation. The above method yields an average $\delta^{18}O_{sw}$ of 0.06‰ for the modern ocean (1950–1984), near the center of the range estimated for this region (−0.1 ± 0.3‰) based on shipboard measurements[53].

At this river-mouth location, seasonal and interannual variability in coral skeletal $\delta^{13}C$ is most influenced by the input of low-$\delta^{13}C$ DIC waters to the coast. While carbon isotopes often reflect multiple influences, including metabolic processes[28,54]; water depth[55]; or the $\delta^{13}C$ of dissolved inorganic carbon (DIC)[56], the coherence between seasonal and interannual river discharge, coral Ba/Ca, and coral $\delta^{13}C$ support the notion that $\delta^{13}C$ of corals at river mouths primarily records river discharge. We made one final modification to the $\delta^{13}C$ values to account for the Suess effect—the change in $\delta^{13}C$ of atmospheric and surface ocean carbon in the 20th century due to the increased combustion of low-$\delta^{13}C$ fossil fuels[57]. Accounting for the Suess effect allows older $\delta^{13}C$ values to be directly compared with the calibration period (1950–1984). To make this adjustment, we added a linear correction of 0.07‰ per decade for the period 1900–1984 to the coral $\delta^{13}C$ values, based on previous estimates[58,59]. Without this small Suess effect correction, average rainfall estimated by $\delta^{13}C$ changes alone would have been ~100 mm/mo lower in the period 1750–1900 and average rainfall estimated by the full multivariate method would have been ~24 mm/mo lower in the same period.

Luminescence

Coral luminescence was originally measured in 0.25 mm intervals, in a line down the center of each coral section. However, the offset between the original luminescence center line and our geochemical transects made direct comparisons challenging. We adopted an alternative approach: using luminescence images of each slab, we digitally extracted color values along each geochemical transect (Supplemental Fig. 1). We then calculated a 7-pt (0.3 mm) running mean of the green-blue ratio to reduce high-frequency noise and interpolated the resulting dataset to 0.75 mm resolution to directly compare luminescence values with the geochemical datasets.

We calculated an annual luminescence value based on either maximum luminescence or the annual range (maximum minus previous minimum) as both are used in previous literature[9,60]. We found that values from either technique are highly correlated with summer rainfall in the calibration period (1950–1984). However, for this study we chose to proceed with the method that uses maximum luminescence for 3 reasons: (1) this core does not appear to exhibit the 'age artifact' that showed declining luminescence intensity with time[60] and which might have made the range method more appropriate, (2) the method is more closely analogous to the method used for calculating peak annual values from the geochemical proxies, and (3) in the older portion of the record (1745–1850), the rainfall estimates based on luminescence are equivalent to those based on the three geochemical proxies only if the 'maximum luminescence' method is used. For this core, rainfall estimates using the range method were typically about half as large in the period 1745–1850 as that calculated via the maximum luminescence method; had this core exhibited the 'age artifact' of selected other cores, luminescence would have instead been greater in this early period.

SEM images

Six samples were collected from locations distributed throughout the core and scanned using a JEOL JSM-7800FLV scanning electron microscope

(SEM) at the University of Michigan's Electron Microbeam Analysis Lab. We used magnifications ranging from 250× to 3000× and all images from this analysis display pristine, primary material, without evidence of diagenesis or overgrowth. See Supplemental Fig. 2 for example images from the core.

Age model

We constructed the age model for this coral using annual cycles in the quasi-sinusoidal Sr/Ca signal. We assigned the coldest sample for each year (highest Sr/Ca) to the month of August, consistent with OISST3v.2 and the high-resolution SST record measured at nearby Lizard Island[61]. If any question remained about the timing of a particular year from the Sr/Ca curve alone, it was resolved by examination of the clear and regular luminescent banding. The resulting average growth rate is 10 ± 2 mm/yr (Supplemental Fig. 4) and the sample resolution is 13 ± 3 samples per year. We then interpolated all records to monthly spacing. Age model and interpolation were performed in the Matlab program Acycle[62].

Instrumental rainfall, river discharge, and ocean temperature

For comparison with coral proxies, we developed regional indices of rainfall and river discharge, using instrumental observations from Australian Bureau of Meteorology stations (rainfall: http://www.bom.gov.au/climate/data/index.shtml; river discharge: http://www.bom.gov.au/waterdata). We derived a rainfall index from 16 stations between 14.5–15.6°S, and river discharge from 6 rivers between 14.9–16°S (Supplemental Fig. 5). Because virtually all precipitation in this region occurs in the summer months, we focus on the wet season, defined as December–April (DJFMA) for rainfall and calculate total DJFMA rainfall for all years. Instrumental rainfall records are not continuous; any year with missing months was discarded and each year contains at least 3 stations that record DJFMA monthly rainfall. For river discharge, we use the period January–April when river flow is highest. We calculated average monthly discharge for January–April after normalizing discharge for each river. The interannual correlation between DJFMA rainfall and normalized regional river discharge is 0.80 ($p < 0.001$) for the overlapping period 1970–1991 that is well-observed ($n \geq 3$ rivers). Local ocean temperature is HadISST (https://www.metoffice.gov.uk/hadobs/hadisst/) for 144–145°E, 14–15°S, 1980–2020.

Rainfall training set and paleo-hydrological calibration

To calibrate interannual rainfall with coral proxies, we summed the 5 months with highest values for the rainy season (DJFMA). For geochemical and luminescence proxies, we interpolated each dataset to monthly resolution and calculated a 3-month running average. We then selected the 'peak' value from each year as the representative value for the rainfall reconstruction (the most positive value for Ba/Ca and luminescence, the most negative value for $\delta^{13}C$, $\delta^{18}O_{sw}$). These extrema occur just after the rainy season: minimum $\delta^{18}O_{sw}$ is in May (±1 month), maximum Ba/Ca and minimum $\delta^{13}C$ are in June (±1 month), and maximum luminescence is in July (±2 months). This approach smooths the data and then looks for local maxima and minima; it is a compromise between an overly smoothed signal that would diminish signal amplitude and an overly noisy signal for which it would be difficult to pick the 'best' annual extreme in each signal. This approach accounts for the fact that hydrologic proxies in coral lag the months of maximum rainfall and accommodates any small (1–2 month) age offsets that are likely present in any coral age model.

Calibration and validation

To test the strength of the rainfall estimation based on coral geochemical analyses, we would ideally validate the results against an independent dataset[63]. However, because few instrumental rainfall observations exist for this region prior to 1950, we cannot validate our 1950–1984 calibration against early 20th century data. As an alternative validation test, we built a test rainfall calibration using only the odd-year data from 1951 to 1983 and validate it using 'independent' even-year data (1950–1984). Vice versa, we also built a rainfall calibration using only even-year data (1950–1984) and validate it using independent odd-year data (1951–1983). Both validation tests of rainfall predicted by the multi-proxy method are significant ($p < 0.001$) when regressed against instrumental rainfall for those years (Supplemental Fig. 7 and Supplemental Table 1.)

Data availability

All original data from this study are publicly available via the National Center for Environmental Information (NCEI) paleoclimatology https://www.ncei.noaa.gov/access/paleo-search/study/38959.

Received: 13 August 2023; Accepted: 7 February 2024;
Published online: 18 March 2024

References

1. Wood, R. R., Lehner, F., Pendergrass, A. G. & Schlunegger, S. Changes in precipitation variability across time scales in multiple global climate model large ensembles. *Environ. Res. Lett.* https://doi.org/10.1088/1748-9326/ac10dd (2021).
2. Pendergrass, A. G., Knutti, R., Lehner, F., Deser, C. & Sanderson, B. M. Precipitation variability increases in a warmer climate. *Sci. Rep.* **7**, 17966 (2017).
3. Westra, S. et al. Future changes to the intensity and frequency of short-duration extreme rainfall. *Rev. Geophys.* **52**, 522–555 (2014).
4. Yun, K.-S. et al. Increasing ENSO–rainfall variability due to changes in future tropical temperature–rainfall relationship. *Commun. Earth Environ.* https://doi.org/10.1038/s43247-021-00108-8 (2021).
5. Grose, M. R. et al. Insights from CMIP6 for Australia's future climate. *Earth's Future* https://doi.org/10.1029/2019ef001469 (2020).
6. Dey, R., Lewis, S. C., Arblaster, J. M. & Abram, N. J. A review of past and projected changes in Australia's rainfall. *WIREs Climate Change* https://doi.org/10.1002/wcc.577 (2019).
7. Lough, J. M. Rainfall variations in Queensland, Australia: 1891-1986. *Int. J. Climatol.* **11**, 745–768 (1991).
8. Nicholls, N., Drosdowsky, W. & Lavery, B. Australian rainfall variability and change. *Weather* **52**, 66–72 (1997).
9. Lough, J. M. Great Barrier Reef coral luminescence reveals rainfall variability over northeastern Australia since the 17th century. *Paleoceanography* https://doi.org/10.1029/2010pa002050 (2011).
10. McCulloch, M. T. et al. Coral record of increased sediment flux to the inner Great Barrier Reef since European settlement. *Nature* **421**, 727–730 (2003).
11. Nicholls, N. Sea surface temperatures and Australian winter rainfall. *J. Clim.* **2**, 965–973 (1989).
12. Risbey, J. S., Pook, M. J., McIntosh, P. C., Wheeler, M. C. & Hendon, H. H. On the remote drivers of rainfall variability in Australia. *Monthly Weather Rev.* **137**, 3233–3253 (2009).
13. Johnson, A. K. L., Ebert, S. P. & Murray, A. E. Distribution of coastal freshwater wetlands and riparian forests in the Herbert River catchment and implications for management of catchments adjacent the Great Barrier Reef Marine Park. *Environ. Conserv.* **26**, 229–235 (1999).
14. Queensland Government. Cape York Region Jeannie catchment water quality targets, https://www.reefplan.qld.gov.au/__data/assets/pdf_file/0017/46043/catchment-targets-cape-york-jeannie.pdf (2019).
15. Sinclair, D. J. & McCulloch, M. T. Corals record low mobile barium concentrations in the Burdekin River during the 1974 flood: evidence for limited Ba supply to rivers? *Palaeogeogr., Palaeoclimatol., Palaeoecol.* **214**, 155–174 (2004).
16. LaVigne, M., Grottoli, A. G., Palardy, J. E. & Sherrell, R. M. Multi-colony calibrations of coral Ba/Ca with a contemporaneous in situ seawater barium record. *Geochim. Cosmochim. Acta* **179**, 203–216 (2016).
17. Lewis, S. E. et al. A critical evaluation of coral Ba/Ca, Mn/Ca and Y/Ca ratios as indicators of terrestrial input: New data from the Great Barrier Reef, Australia. *Geochim. Cosmochim. Acta* **237**, 131–154 (2018).

18. Alibert, C. et al. Source of trace element variability in Great Barrier Reef corals affected by the Burdekin flood plumes. *Geochim. Cosmochim. Acta* **67**, 231–246 (2003).
19. Lea, D. W., Shen, G. T. & Boyle, E. A. Coralline barium records temporal variability in equatorial Pacific upwelling. *Nature* **340**, 373–376 (1989).
20. Sinclair, D. J. Non-river flood barium signals in the skeletons of corals from coastal Queensland, Australia. *Earth Planet. Sci. Lett.* **237**, 354–369 (2005).
21. Grove, C. A. et al. River runoff reconstructions from novel spectral luminescence scanning of massive coral skeletons. *Coral Reefs* **29**, 579–591 (2010).
22. Isdale, P. J. Fluorescent bands in massive corals record centuries of coastal rainfall. *Nature* **310**, 578–579 (1984).
23. Susic, M., Boto, K. & Isdale, P. J. Fluorescent humic acid bands in coral skeletons originate from terrestrial runoff. *Mar. Chem.* **33**, 91–104 (1991).
24. Lough, J. M., Barnes, D. & McAllister, F. Luminescent lines in corals from the Great Barrier Reef provide spatial and temporal records of reefs affected by land runoff. *Coral Reefs* **21**, 333–343 (2002).
25. Alin, S. R., Aalto, R., Goni, M. A., Richey, J. E. & Dietrich, W. E. Biogeochemical characterization of carbon sources in the Strickland and Fly rivers, Papua New Guinea. *J. Geophys. Res*. https://doi.org/10.1029/2006jf000625 (2008).
26. Rosentreter, J. A. & Eyre, B. D. Alkalinity and dissolved inorganic carbon exports from tropical and subtropical river catchments discharging to the Great Barrier Reef, Australia. *Hydrol. Process.* **34**, 1530–1544 (2019).
27. Moyer, R. P., Grottoli, A. G. & Olesik, J. W. A multiproxy record of terrestrial inputs to the coastal ocean using minor and trace elements (Ba/Ca, Mn/Ca, Y/Ca) and carbon isotopes ($\delta^{13}C$, $\Delta^{14}C$) in a nearshore coral from Puerto Rico. *Paleoceanography* https://doi.org/10.1029/2011pa002249 (2012).
28. Grottoli, A. G. & Wellington, G. M. Effect of light and zooplankton on skeletal $\delta^{13}C$ values in the eastern Pacific corals *Pavona clavus* and *Pavona gigantea*. *Coral Reefs* **18**, 29–41 (1999).
29. Hendy, E. J. et al. Abrupt ropical Pacific Sea surface salinity at end of little ice age. *Science* https://doi.org/10.1126/science.1067693 (2002).
30. McCulloch, M. T., Gagan, M. K., Mortimer, G. E., Chivas, A. R. & Isdale, P. J. A high-resolution Sr/Ca and $\delta^{18}O$ coral record from the Great Barrier Reef, Australia, and the 1982-1983 El Niño. *Geochim. Cosmochim. Acta* **58**, 2747–2754 (1994).
31. Ren, L., Linsley, B. K., Wellington, G. M., Schrag, D. P. & Hoegh-Guldberg, O. Deconvolving the $\delta^{18}O$ seawater component from subseasonal coral $\delta^{18}O$ and Sr/Ca at Rarotonga in the southwestern subtropical Pacific for the period 1726 to 1997. *Geochim. Cosmochim. Acta* **67**, 1609–1621 (2003).
32. Jones, D. A., Wang, W. & Fawcett, R. High-quality spatial climate data-sets for Australia. *Aust. Meteorol. Oceanogr. J.* **58**, 233–248 (2009).
33. Ummenhofer, C. C. et al. How did ocean warming affect Australian rainfall extremes during the 2010/2011 La Niña event? *Geophys. Res. Lett.* **42**, 9942–9951 (2015).
34. Allan, R. P. et al. Advances in understanding large-scale responses of the water cycle to climate change. *Ann. N. Y. Acad. Sci.* **1472**, 49–75 (2020).
35. Smith, I. An assessment of recent trends in Australian rainfall. *Aust. Meteorol. Mag.* **53**, 163–173 (2004).
36. Morice, C. P. et al. An updated assessment of near-surface temperature change from 1850: The HadCRUT5 Data Set. *J. Geophys. Res.: Atmos.* https://doi.org/10.1029/2019jd032361 (2021).
37. Emile-Geay, J., Cobb, K. M., Mann, M. E. & Wittenberg, A. T. Estimating Central Equatorial Pacific SST Variability over the Past Millennium. Part II: Reconstructions and Implications. *J. Clim.* **26**, 2329–2352 (2013).
38. Loope, G., Thompson, D., Cole, J. & Overpeck, J. Is there a low-frequency bias in multiproxy reconstructions of tropical Pacific SST variability? *Quat. Sci. Rev*. https://doi.org/10.1016/j.quascirev.2020.106530 (2020).
39. Cai, W. et al. Changing El Niño–Southern Oscillation in a warming climate. *Nat. Rev. Earth Environ.* **2**, 628–644 (2021).
40. Chen, C., Cane, M. A., Wittenberg, A. T. & Chen, D. ENSO in the CMIP5 simulations: life cycles, diversity, and responses to climate change. *J. Clim.* **30**, 775–801 (2017).
41. Power, S. et al. Decadal climate variability in the tropical Pacific: Characteristics, causes, predictability, and prospects. *Science* https://doi.org/10.1126/science.aay9165 (2021).
42. Rodriguez-Ramirez, A., Grove, C. A., Zinke, J., Pandolfi, J. M. & Zhao, J. X. Coral luminescence identifies the Pacific Decadal Oscillation as a primary driver of river runoff variability impacting the southern Great Barrier Reef. *PLoS ONE*. https://doi.org/10.1371/journal.pone.0084305 (2014).
43. Brown, J. R. et al. South Pacific Convergence Zone dynamics, variability and impacts in a changing climate. *Nat. Rev. Earth Environ.* **1**, 530–543 (2020).
44. DeLong, K. L., Quinn, T. M., Taylor, F. W., Lin, K. & Shen, C.-C. Sea surface temperature variability in the southwest tropical Pacific since AD 1649. *Nat. Clim. Change* **2**, 799–804 (2012).
45. Linsley, B. K. et al. Tracking the extent of the South Pacific Convergence Zone since the early 1600s. *Geochem. Geophys. Geosyst*. https://doi.org/10.1029/2005gc001115 (2006).
46. Tierney, J. E. et al. Tropical sea-surface temperatures for the past four centuries reconstructed from coral archives. *Paleoceanography* https://doi.org/10.1002/2014PA002717 (2015).
47. Lough, J. M., Lewis, S. E. & Cantin, N. E. Freshwater impacts in the central Great Barrier Reef: 1648–2011. *Coral Reefs* **34**, 739–751 (2015).
48. Lough, J. M., Barnes, D. J., Devereux, M. J., Tobin, B. J. & Tobin, S. *Variability in growth characteristics of massive Porites on the Great Barrier Reef*. 28 (James Cook University, 1999).
49. Cantarero, S. I., Tanzil, J. T. I. & Goodkin, N. F. Simultaneous analysis of Ba and Sr to Ca ratios in scleractinian corals by inductively coupled plasma optical emissions spectrometry. *Limnol. Oceanogr.: Methods* **15**, 116–123 (2016).
50. Schrag, D. P. Rapid analysis of high-precision Sr/Ca ratios in corals and other marine carbonates. *Paleoceanography* **14**, 97–102 (1999).
51. Hathorne, E. C. et al. Interlaboratory study for coral Sr/Ca and other element/Ca ratio measurements. *Geochem. Geophys. Geosyst.* **14**, 3730–3750 (2013).
52. Brenner, L. D., Linsley, B. K. & Potts, D. C. A modern Sr/Ca-$\delta^{18}O$-sea surface temperature calibration for *Isopora* corals on the Great Barrier Reef. *Paleoceanography* **32**, 182–194 (2017).
53. Munksgaard, N. C., Wurster, C. M., Bass, A., Zagorskis, I. & Bird, M. I. First continuous shipboard $\delta^{18}O$ and δD measurements in sea water by diffusion sampling—cavity ring-down spectrometry. *Environ. Chem. Lett.* **10**, 301–307 (2012).
54. McConnaughey, T. A., Burdett, J., Whelan, J. F. & Paull, C. K. Carbon isotopes in biological carbonates: Respiration and photosynthesis. *Geochim. Cosmochim. Acta* **61**, 611–622 (1997).
55. Linsley, B. K. et al. Coral carbon isotope sensitivity to growth rate and water depth with paleo-sea level implications. *Nat. Commun.* **10**, 1–9 (2019).
56. Moyer, R. P. & Grottoli, A. G. Coral skeletal carbon isotopes ($\delta^{13}C$ and $\Delta^{14}C$) record the delivery of terrestrial carbon to the coastal waters of Puerto Rico. *Coral Reefs* https://doi.org/10.1007/s00338-011-0758-y (2011).
57. Swart, P. K. et al. The stable oxygen and carbon isotopic record from a coral growing in Florida Bay: a 160 year record of climatic and anthropogenic influence. *Palaeogeogr., Palaeoclimatol., Palaeoecol.* **123**, 219–237 (1996).

58. Druffel, E. R. M. & Benavides, L. M. Input of excess CO_2 to the surface ocean based on $^{13}C/^{12}C$ ratios in a banded Jamaican sclerosponge. *Nature* https://doi.org/10.1038/321058a0 (1986).
59. Dassié, E. P., Lemley, G. M. & Linsley, B. K. The Suess effect in Fiji coral $\delta^{13}C$ and its potential as a tracer of anthropogenic CO_2 uptake. *Palaeogeogr., Palaeoclimatol., Palaeoecol.* **370**, 30–40 (2013).
60. Isdale, P. J., Stewart, B. J., Tickle, K. S. & Lough, J. M. Palaeohydrological variation in a tropical river catchment: a reconstruction using fluorescent bands in corals of the Great Barrier Reef, Australia. *Holocene* https://doi.org/10.1191/095968398670905088 (1998).
61. Anderson, K. D., Cantin, N. E., Heron, S. F., Pisapia, C. & Pratchett, M. S. Variation in growth rates of branching corals along Australia's Great Barrier Reef. *Sci. Rep.* **7**, 2920 (2017).
62. Li, M., Hinnov, L. & Kump, L. Acycle: Time-series analysis software for paleoclimate research and education. *Computers Geosci.* **127**, 12–22 (2019).
63. Crowley, T. J., Quinn, T. M. & Hyde, W. T. Validation of coral temperature calibrations. *Paleoceanography* **14**, 605–615 (1999).
64. Reed, E. V., Cole, J. E., Lough, J. M., Thompson, D. & Cantin, N. E. Linking climate variability and growth in coral skeletal records from the Great Barrier Reef. *Coral Reefs* **38**, 29–43 (2018).
65. Jourdain, N. C. et al. The Indo-Australian monsoon and its relationship to ENSO and IOD in reanalysis data and the CMIP3/CMIP5 simulations. *Clim. Dyn.* **41**, 3073–3102 (2013).
66. Trouet, V. & Van Oldenborgh, G. J. KNMI climate explorer: a web-based research tool for high-resolution paleoclimatology. *Tree-Ring Res.* **69**, 3–13 (2013).
67. Neukom, R. et al. Consistent multidecadal variability in global temperature reconstructions and simulations over the Common Era. *Nat. Geosci.* **12**, 1–11 (2019).

Acknowledgements

We respectfully acknowledge the Traditional Custodians of the land and sea Country surrounding the Jeannie River and recognize Aboriginal and Torres Strait Islander people as Australia's first scientists. We gratefully thank AIMS for preserving and providing the coral material analyzed herein. This work was funded in part by NSF through the OCE Marine Geology and Geophysics program, grant #1851587 to J.E.C.

Author contributions

K.A.D. coordinated the project, led data collection/curation and initial draft writing, and contributed to the project conceptualization, method development, data analysis and interpretation, and visualizations. J.E.C. conceived the project ideas, acquired financial support, and contributed to method development, data interpretation, and draft manuscript writing. J.M.L. provided study materials and contributed to project conceptualization and data interpretation. All authors contributed critical review and revisions of manuscript drafts, including the final version.

Competing interests

The authors declare no competing interests.

Additional information

Supplementary information The online version contains supplementary material available at https://doi.org/10.1038/s43247-024-01262-5.

Correspondence and requests for materials should be addressed to Kelsey A. Dyez.

Peer review information *Communications Earth & Environment* thanks the anonymous reviewers for their contribution to the peer review of this work. Primary Handling Editors: Yama Dixit, Joe Aslin, Clare Davis and Martina Grecequet. A peer review file is available.